



**UvA-DARE (Digital Academic Repository)**

**Tomographic Separation of Composite Spectra. VII. The Physical Properties of the Massive Triple System**

Penny, L.R.; Seyle, D.; Gies, D.R.; Harvin, J.A.; Bagnuolo, W.G.; Thaller, M.L.; Fullerton, A.W.; Kaper, L.

*Published in:*  
Astrophysical Journal

*DOI:*  
[10.1086/319031](https://doi.org/10.1086/319031)

[Link to publication](#)

*Citation for published version (APA):*

Penny, L. R., Seyle, D., Gies, D. R., Harvin, J. A., Bagnuolo, W. G., Thaller, M. L., ... Kaper, L. (2001). Tomographic Separation of Composite Spectra. VII. The Physical Properties of the Massive Triple System. *Astrophysical Journal*, 548, 889-899. DOI: 10.1086/319031

**General rights**

It is not permitted to download or to forward/distribute the text or part of it without the consent of the author(s) and/or copyright holder(s), other than for strictly personal, individual use, unless the work is under an open content license (like Creative Commons).

**Disclaimer/Complaints regulations**

If you believe that digital publication of certain material infringes any of your rights or (privacy) interests, please let the Library know, stating your reasons. In case of a legitimate complaint, the Library will make the material inaccessible and/or remove it from the website. Please Ask the Library: <http://uba.uva.nl/en/contact>, or a letter to: Library of the University of Amsterdam, Secretariat, Singel 425, 1012 WP Amsterdam, The Netherlands. You will be contacted as soon as possible.

## TOMOGRAPHIC SEPARATION OF COMPOSITE SPECTRA. VII. THE PHYSICAL PROPERTIES OF THE MASSIVE TRIPLE SYSTEM HD 135240 ( $\delta$ CIRCINI)

LAURA R. PENNY<sup>1</sup> AND DEBRA SEYLE

Department of Physics and Astronomy, College of Charleston, 66 George Street, Charleston, SC 29424; penny@cofc.edu, seyled@edisto.cofc.edu

DOUGLAS R. GIES,<sup>1</sup> JAMES A. HARVIN, AND WILLIAM G. BAGNUOLO, JR.<sup>1</sup>

Center for High Angular Resolution Astronomy and Department of Physics and Astronomy, Georgia State University, Atlanta, GA 30303; gies@chara.gsu.edu, harvin@chara.gsu.edu, bagnuolo@chara.gsu.edu

M. L. THALLER<sup>2</sup>

Infrared Processing and Analysis Center, California Institute of Technology and Jet Propulsion Laboratory, Pasadena, CA 91125; thaller@ipac.caltech.edu

A. W. FULLERTON<sup>3</sup>

Department of Physics and Astronomy, University of Victoria, Victoria, BC V8W 3P6, Canada; awf@pha.jhu.edu

AND

L. KAPER

Sterrenkundig Instituut “Anton Pannekoek,” University of Amsterdam, Kruislaan 403 1098 SJ, Amsterdam, Netherlands; lexk@astro.uva.nl

Received 2000 September 22; accepted 2000 October 18

### ABSTRACT

We present the results of a radial velocity study of the massive, double-lined, O binary HD 135240 based primarily on UV spectroscopy from the *International Ultraviolet Explorer*. Cross-correlation methods indicate the presence of a third stationary spectral line component which indicates that the system is a triple consisting of a central 3.9 day close binary with a distant companion. We measured radial velocities from the cross-correlation functions after removal of the third component, and we combined these with velocities obtained from H $\alpha$  spectroscopy to reassess the orbital elements. We applied a Doppler tomography algorithm to reconstruct the individual UV spectra of all three stars, and we determine spectral classifications of O7 III–V, O9.5 V, and B0.5 V for the primary, secondary, and tertiary, respectively, using UV criteria defined by Penny, Gies, & Bagnuolo. We compare these reconstructed spectra to standard single-star spectra to find the UV flux ratios of the components ( $F_2/F_1 = 0.239 \pm 0.022$ , and  $F_3/F_1 = 0.179 \pm 0.021$ ). *Hipparcos* photometry reveals that the central pair is an eclipsing binary, and we present the first model fit of the light curve from which we derive an orbital inclination,  $i = 74^\circ \pm 3^\circ$ . This analysis indicates that neither star is currently experiencing Roche lobe overflow. We place the individual components in the theoretical H-R diagram, and we show that the masses derived from the combined spectroscopic and photometric analysis ( $M_p/M_\odot = 21.6 \pm 2.0$  and  $M_s/M_\odot = 12.4 \pm 1.0$ ) are significantly lower than those computed from evolutionary tracks for single stars.

*Subject headings:* binaries: eclipsing — binaries: spectroscopic — stars: early-type — stars: fundamental parameters — stars: individual (HD 135240) — ultraviolet: stars

### 1. INTRODUCTION

In this series of papers we have attempted to utilize the tomography algorithm to better study the individual stars that make up multiple systems. Our targets have included AO Cassiopeiae (Bagnuolo & Gies 1991), Plaskett’s Star (Bagnuolo, Gies, & Wiggs 1992), 29 UW Canis Majoris (Bagnuolo et al. 1994),  $\phi$  Persei (Thaller et al. 1995), DH Cephei (Penny, Gies, & Bagnuolo 1997), and HD 152248 (Penny, Gies, & Bagnuolo 1999).

This time we turn our attention to the close, massive binary system HD 135240 ( $\delta$  Circini). This system is particularly interesting to us because of the discovery by *Hipparcos* of its eclipsing light curve (Perryman 1997). Thackeray & Emerson (1969) published a single-lined orbital solution with an estimate of the mass ratio from a few observations of the secondary’s He I lines. Intriguingly enough, they discussed an unpublished photometric light curve made by Cousins which displayed two shallow minima of about 0.1

mag in  $V$ . Stickland et al. (1993, hereafter ST93) utilized the majority of *International Ultraviolet Explorer* (*IUE*) spectra that we present here to determine the first double-lined solution. Their observations of the secondary’s UV photospheric lines greatly improved on the orbital solution and mass ratio. However, they dismissed the reports of possible eclipses as probably attributable to ellipsoidal (tidal) variations of the stars.

This system highlights one of the common problems with close, massive, double-lined spectroscopic binaries. Despite the excellent orbital solution presented by ST93, only the minimum masses and orbital separation are determined. Estimates of the true values are dependent on the assumed inclination of the orbit to the plane of the sky. This is usually a frustrating situation, since the most interesting parameters are arguably the masses and separation (and hence, degree of interaction). The discovery of an eclipsing light curve is very exciting since the depths and durations of the eclipses are sensitive functions of both the inclination and radii of the stars, and numerical modeling of the light curve can lead to better estimates of the masses and separation.

In this paper we present our own analysis of the *IUE* observations of HD 135240, which we find to be a triple-

<sup>1</sup> Guest Observer with the *International Ultraviolet Explorer* satellite.

<sup>2</sup> Visiting Astronomer, Mount Stromlo Observatory.

<sup>3</sup> Postal address: FUSE Science Center, Department of Physics and Astronomy, Johns Hopkins University, 3400 North Charles Street, Baltimore, MD 21218.

lined system (§ 2). We present radial velocities derived from the *IUE* spectra and H $\alpha$  spectroscopy, which we use to revise the orbital elements (§ 4). We determine individual projected rotational velocities (§ 5), and we apply a Doppler tomography analysis to reconstruct the separate component spectra and determine their spectral classifications (§ 6). Our model of the eclipsing light curve (§ 7) leads directly to mass estimates which we compare with masses from evolutionary tracks of single stars (§ 8).

## 2. *IUE* OBSERVATIONS AND CROSS-CORRELATION VELOCITIES

There are 41 high-dispersion, short wavelength prime (SWP) camera spectra of HD 135240 available from *IUE*. Twenty-nine of these spectra were obtained in 1992 September in an international campaign to improve the fundamental parameters of massive close binaries (ST93). The individual SWP image numbers and heliocentric Julian dates of midexposure are presented in Table 1. The spectra

were obtained in NEWSIPS format (Garhart et al. 1997) from the Multimission Archive at the Space Telescope Science Institute,<sup>4</sup> and these spectra were subsequently manipulated in several stages to produce a matrix of spectra (in dimensions of wavelength and time) rectified using a common set of relatively line-free zones and sampled with a uniform log  $\lambda$  wavelength grid. The major interstellar absorption lines were replaced by straight line segments in the processing. Details are given in Penny et al. (1997).

Radial velocities derived from 37 of these spectra are presented by ST93. However, we decided to check their results using our suite of cross-correlation techniques to obtain radial velocities and estimates of projected rotational velocities (see Penny et al. 1997 for details). We followed the example of ST93 by selecting the narrow-lined spectrum of  $\tau$  Sco (HD 149438; B0.2 V; projected rotational velocity,  $v \sin i < 5 \text{ km s}^{-1}$ ; Hardorp & Scholz 1970; Slettebak et al.

<sup>4</sup> Available at <http://archive.stsci.edu/iue>.

TABLE 1  
*IUE* RADIAL VELOCITY MEASUREMENTS

SWP Image	HJD (-2,400,000)	Orbital Phase	$V_1$ ( $\text{km s}^{-1}$ )	$(O-C)_1$ ( $\text{km s}^{-1}$ )	$W_1$	$V_2$ ( $\text{km s}^{-1}$ )	$(O-C)_2$ ( $\text{km s}^{-1}$ )	$W_2$
2494	43,756.9160	0.1210	127.0	7.4	1.0	-169.3	41.2	1.0
2495	43,756.9465	0.1288	132.6	8.4	1.0	-186.6	32.0	1.0
6146	44,096.2403	0.0720	86.4	3.2	1.0	-147.2	-0.6	1.0
6394	44,121.8638	0.6379	-134.0	-10.7	1.0	211.6	-3.9	1.0
9617	44,449.0274	0.4728	28.4	24.6	0.0	20.7	28.2	0.0
9634	44,450.2738	0.7922	-140.3	10.8	1.0	282.8	18.6	1.0
9674	44,454.1668	0.7898	-137.9	13.8	1.0	291.4	26.1	1.0
9740	44,460.2479	0.3480	146.9	44.1	0.0	-184.9	-4.0	1.0
45679	48,885.1509	0.2187	143.5	-5.7	1.0	-256.1	6.3	1.0
45682	48,885.2712	0.2495	140.5	-5.6	1.0	-251.1	5.8	1.0
45685	48,885.3794	0.2772	131.1	-7.5	1.0	-236.8	7.0	1.0
45691	48,885.8688	0.4027	66.9	3.9	1.0	-114.6	-3.4	1.0
45692	48,885.8911	0.4084	64.3	5.9	1.0	-101.0	2.2	1.0
45695	48,885.9847	0.4324	42.9	4.3	1.0	-67.3	1.2	1.0
45696	48,886.0053	0.4376	34.7	0.5	1.0	-77.2	-16.6	1.0
45699	48,886.0873	0.4586	10.8	-5.3	0.0	-35.8	-6.8	0.0
45700	48,886.1066	0.4636	0.8	-11.1	0.0	-46.0	-24.5	0.0
45703	48,886.3819	0.5341	-39.5	9.3	1.0	109.9	25.0	1.0
45706	48,886.4756	0.5581	-59.3	9.1	1.0	148.4	29.3	1.0
45707	48,886.4978	0.5638	-64.8	8.0	1.0	130.3	3.3	1.0
45713	48,886.7216	0.6212	-114.5	-1.1	1.0	187.8	-10.3	1.0
45714	48,886.7431	0.6267	-120.1	-3.3	1.0	204.5	0.5	1.0
45717	48,886.8313	0.6493	-132.6	-3.2	1.0	214.1	-12.1	1.0
45718	48,886.8535	0.6550	-136.3	-4.0	1.0	216.5	-14.7	1.0
45721	48,886.9418	0.6776	-145.7	-3.5	1.0	244.8	-3.9	1.0
45722	48,886.9647	0.6835	-151.5	-7.1	1.0	237.0	-15.5	1.0
45725	48,887.0508	0.7055	-165.4	-14.2	1.0	258.2	-6.1	1.0
45726	48,887.0754	0.7118	-160.0	-7.4	1.0	248.0	-18.8	1.0
45728	48,887.1499	0.7309	-162.8	-7.1	1.0	256.2	-16.0	1.0
45730	48,887.2243	0.7500	-165.3	-8.6	1.0	271.2	-2.8	1.0
45732	48,887.2859	0.7658	-163.9	-8.0	1.0	261.3	-11.3	1.0
45734	48,887.3681	0.7868	-158.5	-6.1	1.0	263.0	-3.5	1.0
45736	48,887.4346	0.8039	-151.6	-4.0	1.0	262.7	4.6	1.0
45745	48,888.3318	0.0338	43.4	-3.9	1.0	-100.4	-16.7	1.0
45747	48,888.3952	0.0500	60.3	-2.9	1.0	-141.0	-29.4	1.0
45749	48,888.4532	0.0649	71.8	-5.2	1.0	-182.6	-46.9	1.0
45793	48,894.3720	0.5816	-83.9	2.5	1.0	161.8	11.2	1.0
47882	49,155.3382	0.4535	22.2	1.7	0.0	61.9	98.7	0.0
48293	49,203.0627	0.6828	-133.2	11.0	1.0	260.6	8.5	1.0
54308	49,813.5280	0.1131	128.2	13.5	1.0	-198.5	3.3	1.0
55814	49,964.9949	0.9261	-55.6	8.7	1.0	147.6	35.5	1.0

1975) as our cross-correlation reference spectrum. We used the same methods to make a spectrum matrix of the last 10 spectra of  $\tau$  Sco from *IUE*, and these were averaged to improve the signal-to-noise ratio (S/N). We then calculated cross-correlation functions (CCFs) of each spectrum of HD 135240 with the reference  $\tau$  Sco spectrum after first setting to unity the spectral regions containing very broadened features. Each CCF was subsequently rectified by fitting a low-order polynomial to its extreme wings.

Inspection of the CCFs immediately showed that the secondary component was readily visible and well separated from the primary in CCFs from phases of large radial velocity difference. However, a closer examination revealed that our usual method of double-Gaussian fitting of the CCFs was doomed to failure in this case. The problem is illustrated in Figure 1, which shows the CCF for SWP 45730 obtained near secondary maximum velocity (*plus signs*). The left-hand panel shows the results of a two-Gaussian fit in which the best fit of the secondary component is both too wide and misplaced to line center due to the excess CCF strength between the components. The addition of a small, central third component (*right-hand panel*) produces satisfactory agreement throughout the CCF. We found this same central filling of the CCF in all the well-separated cases.

The simplest explanation for the third component is that it originates in a third distant star which orbits the close binary with a minimum period measured in decades. The orbital motion of the third star would then show little or no change over the duration of the *IUE* spectra. There is no indication of an astrometric companion either in the *Hipparcos* results or in speckle observations (Mason et al.

1998), but we suspect that future high-resolution observations will find the companion.

Preliminary tests using three-Gaussian fits for all the CCFs resulted in unstable solutions except in the well-separated cases. Instead, we decided to make a more constrained fit by first removing the central component from all the CCFs. We began by making three-Gaussian fits of the 15 best separated CCFs using the deblending procedure in the IRAF<sup>5</sup> routine “splot.” These were unconstrained fits of Gaussian equivalent width, FWHM, and central position, and they generally produced consistent results for these parameters for each of the primary, secondary, and tertiary. The average fitted FWHM is  $218 \pm 10$ ,  $202 \pm 23$ , and  $192 \pm 34$  km s<sup>-1</sup> for these components, respectively. We found no evidence of significant positional changes in the third component in these 15 CCFs. We therefore took the average parameters for the third component (centered at a midrange radial velocity of  $+16$  km s<sup>-1</sup>) and subtracted this constant Gaussian component from all the CCFs. The resulting CCFs are illustrated in Figure 2.

The CCFs after removal of the third component were then fitted with the reliable double-Gaussian fitting procedure. We fixed the Gaussian widths to the FWHM given above for the well-separated cases. In our prior work we also constrained the intensity ratio (secondary to primary peak ratio) in making a two-Gaussian fit, but here we abandon this constraint. Figure 2 shows that the secondary

<sup>5</sup> IRAF is distributed by the National Optical Astronomy Observatories, which is operated by the Association of Universities for Research in Astronomy, Inc., under contract to the National Science Foundation.

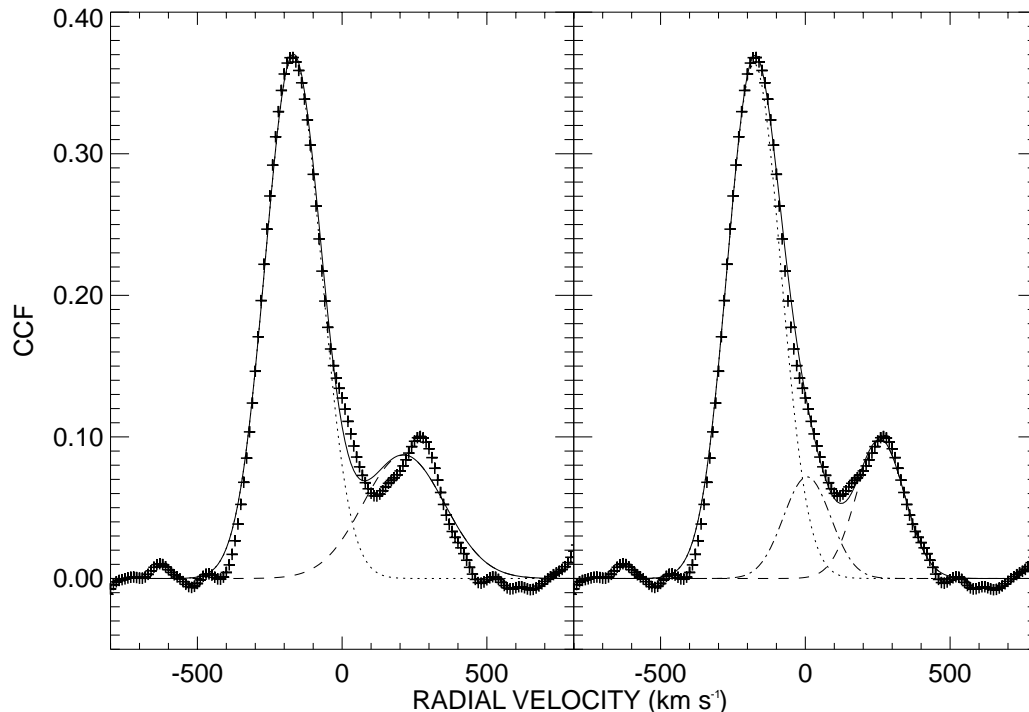


FIG. 1.—CCF for SWP45730 at a phase where the primary and secondary components are well resolved (*plus signs*). The left-hand panel shows the results of a two-Gaussian fit (*primary: dotted line; secondary: dashed line; sum: solid line*) in which the secondary component fit is both too broad and too close to line center due to the extra CCF strength between components. A three-Gaussian fit (*right*) including a central component (*dot-dashed line*) makes a much better fit.

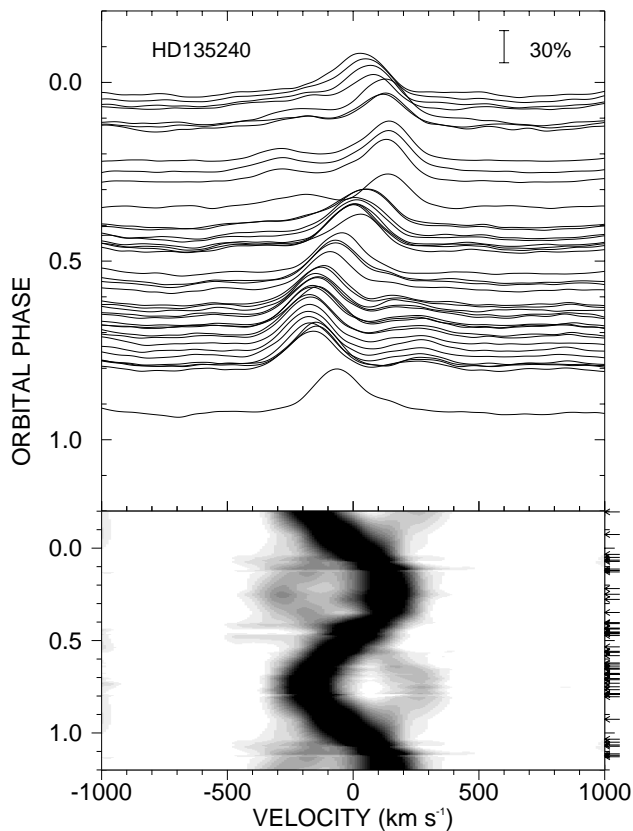


FIG. 2.—*Top*: Cross-correlation functions of *IUE* spectra of HD 135240 with that of the reference star, HD 149438 (after removal of a central Gaussian component) plotted against heliocentric radial velocity. The profiles are arranged in order of increasing orbital phase and each function is placed in the *y*-ordinate so that the continuum equals the phase of observation. *Bottom*: Reverse gray-scale representation of the functions above. The profile at each phase is calculated by a linear interpolation between the closest observed phases (marked by arrows on the right-hand side). To improve the sense of phase continuity, the first and last 20% of the orbit have been reproduced at the bottom and top of the image, respectively.

component appears stronger during approaching phases compared to receding phases, a phenomenon observed in many massive binaries and known as the “Struve-Sahade effect” (Gies, Bagnuolo, & Penny 1997; Howarth et al. 1997; Stickland 1997), so we let the component intensities be free parameters in each CCF fit. The resulting fitted positions of the components are presented in Table 1 after transformation from relative to absolute velocity by adding the radial velocity of  $\tau$  Sco ( $+2.0 \text{ km s}^{-1}$ ; Stickland et al. 1992).

### 3. $H\alpha$ OBSERVATIONS AND RADIAL VELOCITIES

The target was also the subject of  $H\alpha$  spectroscopy in independent projects to search for evidence of colliding winds (Thaller 1997) and to study periodic variations at the base of the wind (Kaper et al. 1998). The  $H\alpha$  line is not ideal for the purposes of measuring radial velocities of binary components because it is strongly Stark broadened (so that the components are not clearly resolved), and it displays weak and variable emission that has its origin in the wind of the primary. Nevertheless, the fact that the secondary was readily evident in these profiles encouraged us to measure radial velocities using double-Gaussian fits. There are 18  $H\alpha$  spectra (made in 1995 by Kaper and Fullerton) from the European Southern Observatory (ESO) Coudé Auxiliary Telescope with the Coudé Echelle Spectrometer using the red-optimized path with CCD 34 ( $2048 \times 2048$  pixels), windowed to 40 pixels in the cross-dispersion direction, as a detector. This arrangement produced a spectral coverage of  $6533\text{--}6594 \text{ \AA}$  with a reciprocal dispersion of  $0.029 \text{ \AA pixel}^{-1}$ , with a typical S/N of  $250 \text{ pixel}^{-1}$ . We also have three  $H\alpha$  spectra (made in 1996 by Thaller) from the 74 inch Telescope at the Mount Stromlo Observatory (MSO) using the coudé spectrograph, grating C ( $600 \text{ grooves mm}^{-1}$ , blazed at  $12500 \text{ \AA}$ ) in second order and the  $81.3 \text{ cm}$  focal length camera. This produced a reciprocal dispersion of  $0.24 \text{ \AA pixel}^{-1}$  on a thinned 2K Tektronix CCD detector

TABLE 2  
 $H\alpha$  RADIAL VELOCITY MEASUREMENTS

HJD ( $-2,400,000$ )	Orbital Phase	$V_1^a$ ( $\text{km s}^{-1}$ )	$(O-C)_1$ ( $\text{km s}^{-1}$ )	$W_1$	$V_2^a$ ( $\text{km s}^{-1}$ )	$(O-C)_2$ ( $\text{km s}^{-1}$ )	$W_2$	Source
49,867.539.....	0.953	-41.3	-4.3	0.0	116.0	51.8	0.0	ESO
49,867.709.....	0.997	21.8	12.7	0.0	...	...	...	ESO
49,868.504.....	0.201	141.1	-7.3	1.0	-268.7	-7.8	1.0	ESO
49,868.644.....	0.236	141.0	-7.1	1.0	-263.4	-2.9	1.0	ESO
49,868.819.....	0.281	136.2	-1.0	1.0	-258.6	-17.3	1.0	ESO
49,869.516.....	0.460	22.1	7.1	0.0	...	...	...	ESO
49,869.622.....	0.487	1.0	9.5	0.0	...	...	...	ESO
49,869.755.....	0.521	-33.4	4.4	1.0	70.2	4.7	1.0	ESO
49,870.519.....	0.717	-142.8	10.8	1.0	278.6	10.0	1.0	ESO
49,870.720.....	0.768	-140.5	15.1	1.0	260.4	-11.7	1.0	ESO
49,871.600.....	0.994	11.5	5.6	0.0	-24.0	-12.9	0.0	ESO
49,871.779.....	0.040	51.7	-1.6	1.0	-78.3	15.9	1.0	ESO
49,872.512.....	0.228	149.2	0.3	1.0	-262.5	-0.6	1.0	ESO
49,872.710.....	0.278	135.2	-3.1	1.0	-263.4	-20.2	1.0	ESO
49,873.520.....	0.486	-4.2	3.3	0.0	...	...	...	ESO
49,873.705.....	0.533	-45.2	2.8	1.0	87.1	3.6	1.0	ESO
49,874.609.....	0.765	-144.6	11.4	1.0	257.8	-14.9	1.0	ESO
49,874.790.....	0.811	-132.7	12.3	1.0	268.9	15.4	1.0	ESO
50,152.141.....	0.882	-124.1	-20.8	1.0	197.0	16.7	1.0	MSO
50,154.179.....	0.404	63.3	1.4	1.0	-111.8	-2.6	1.0	MSO
50,155.082.....	0.635	-141.1	-19.2	1.0	199.7	-13.4	1.0	MSO

<sup>a</sup> Corrected to a revised zero point. See § 4.

TABLE 3  
ORBITAL ELEMENTS

Parameter	ST93	Combined	Primary Only	Secondary Only
$P$ (days) .....	3.902456 (fixed)	3.902476(21)	3.902519(29)	3.902428(31)
$T$ ( $HJD - 2,400,000$ ) .....	48884.285(57)	49871.624(7)	49871.36(18)	49871.72(11)
$K_1$ ( $\text{km s}^{-1}$ ) .....	148.8(1.3)	153.0(1.4)	151.6(1.5)	...
$K_2$ ( $\text{km s}^{-1}$ ) .....	257.4(1.9)	268.2(2.8)	...	270.2(3.1)
$e$ .....	0.061(6)	0.051(8)	0.041(10)	0.068(13)
$\omega$ (deg) .....	274.4(5.3)	276.0(8.5)	251(16)	286 + 180(10)
$V_0$ ( $\text{km s}^{-1}$ ) .....	-17.8(1.0)	...	...	...
$V_{0,1}$ ( $\text{km s}^{-1}$ ) .....	...	-4.5(1.1)	-4.3(1.2)	...
$V_{0,2}$ ( $\text{km s}^{-1}$ ) .....	...	7.2(2.2)	...	8.4(2.4)
$m_1 \sin^3 i$ ( $M_\odot$ ) .....	17.09(23)	19.2(6)	...	...
$m_2 \sin^3 i$ ( $M_\odot$ ) .....	9.88(14)	11.0(3)	...	...
$a_1 \sin i$ ( $R_\odot$ ) .....	11.44(10)	11.78(11)	11.67(11)	...
$a_2 \sin i$ ( $R_\odot$ ) .....	19.81(15)	20.65(22)	...	20.78(24)
rms ( $\text{km s}^{-1}$ ) .....	6.4	...	...	...
rms <sub>1</sub> ( $\text{km s}^{-1}$ ) .....	...	8.5	8.2	...
rms <sub>2</sub> ( $\text{km s}^{-1}$ ) .....	...	16.8	...	17.0

(2KCCD). An RG610 filter was used to block the higher order light. All these spectra were reduced using standard techniques that included removal of atmospheric telluric lines.

The radial velocities for H $\alpha$  were measured in the same way as done with the IUE CCFs, i.e., by first estimating the component widths in well-separated spectra and then fixing these widths by fitting Gaussians to the entire set of profiles. Because of the large Stark broadening present, there was no reliable way to measure the strength of the third component (Fig. 1) since this component was always fully blended with the primary component. Instead, we made only double-Gaussian fits that ignored the central component. This

omission probably means that our measurements at the velocity extrema slightly underestimate the true velocities since these fits try to accommodate the (unknown) line contribution of the third component near line center. We made a simple test by subtracting from the profile centers the Gaussian profile used for the secondary prorated by the tertiary to secondary  $V$ -band flux ratio (§ 7) and then remeasuring velocities in these “tertiary-free” profiles. This test indicates that our H $\alpha$  radial velocities may underestimate the actual secondary semiamplitude by as much as 20  $\text{km s}^{-1}$ . Nevertheless, we present the simple, double-Gaussian fitted velocities in Table 2, since attempts to “correct” the H $\alpha$  profiles for the tertiary would introduce

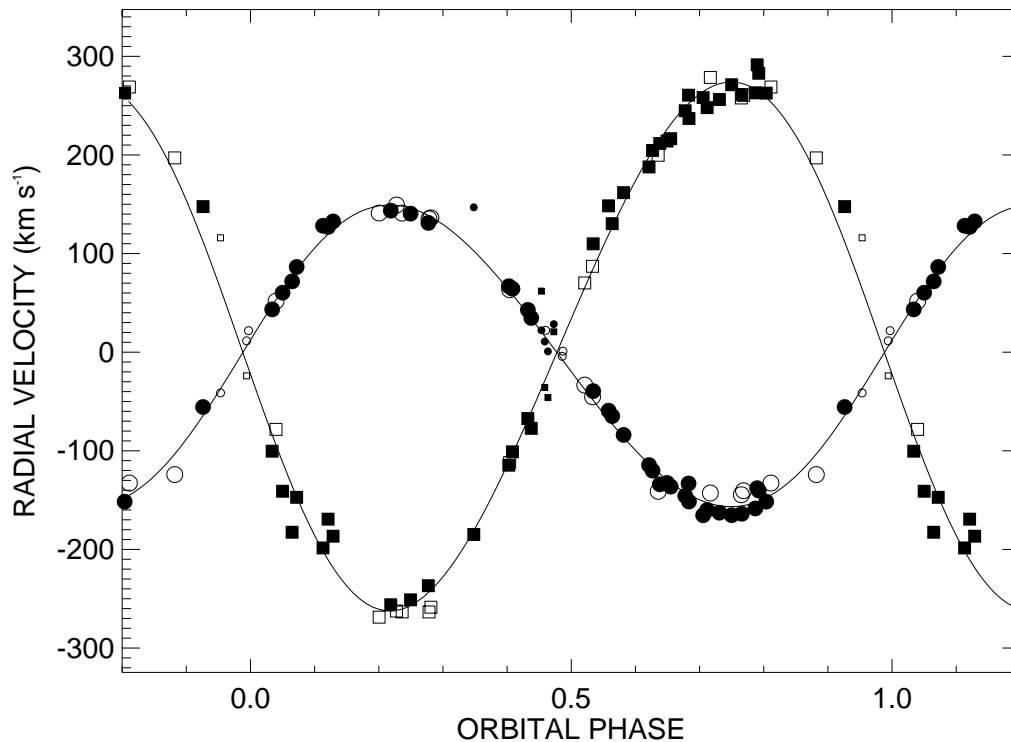


FIG. 3.—Radial velocity measurements for the primary (circles) and secondary (squares) based on the UV CCFs (filled symbols) and H $\alpha$  profiles (open symbols). Smaller symbols represent data assigned zero weight in the orbital solutions. Solid lines are drawn for both the primary and secondary radial velocity solutions.

other systematic errors dependent on the poorly known tertiary contribution to the composite profile.

#### 4. REVISED ORBITAL ELEMENTS

The radial velocity data presented in §§ 2 and 3 were combined to reassess the orbital elements. The atmospheres of massive stars are in a state of expansion which progresses from near stability deep in the photosphere to supersonic outflow in the wind, and the radial velocities of lines formed at different depths in the atmosphere will reflect the local motion (Hutchings 1976; Bohannan & Garmany 1978). Thus, we expect to find differences in the binary systemic velocity derived from H $\alpha$  (high in atmosphere) and the UV CCFs (representing high-excitation lines formed deeper in the atmosphere). Similarly, we also expect to find differences between the systemic velocities of the primary and secondary stars since the former possesses a much more energetic wind. We solved for the elements in an iterative manner that accounted for these potential differences. We first used the period found by ST93 to determine the orbital elements from the combined UV CCF and H $\alpha$  data using the program (SBCM) of Morbey & Brosterhus (1974). Individual solutions were determined for both component stars, and data obtained near eclipse phases (§ 7) were assigned zero weight (indicated by  $\bar{W}$  in Tables 1 and 2). We then used these solutions to make separate fits of the UV CCF and H $\alpha$  measurements by fixing all the elements except the systemic velocity. The resulting systemic velocity was 19.6 (16.0) km s $^{-1}$  lower for the H $\alpha$  velocities of the primary (secondary), so we added these offsets to the H $\alpha$  velocities to place them on the same system as the UV CCF velocities (the data quoted in Table 2 include these offsets). We next determined all the orbital elements from the combined and corrected velocity measurements. These are listed in Table 3 for both the primary and secondary. Finally, we created a combined solution by forming the error-weighted averages of all the elements common to the primary and secondary (period  $P$ , epoch of periastron  $T$ , eccentricity  $e$ , and longitude of periastron  $\omega$ ), and, having set these elements, we solved for the individual semiamplitudes,  $K$ , and systemic velocities,  $V_0$ . This combined solution is also given in Table 3, and it is used to define orbital phase throughout this paper. The combined primary and secondary solution of ST93 is also presented in Table 3. The numbers in parentheses refer to the errors in the last digit quoted.

The results of the combined solution are shown in the radial velocity curve in Figure 3. There is good agreement between velocities from the UV CCFs (*filled symbols*) and from H $\alpha$  (*open symbols*) over most of the orbit. The H $\alpha$  primary measurements near primary minimum velocity appear to underestimate the motion (as expected because of blending with the tertiary profile; § 3), but the differences are comparable to the measurement errors. Most of the revised elements agree well with those from ST93 with the exceptions of the semiamplitudes and systemic velocity. We suspect that these differences are due to the presence of the tertiary which was unaccounted for in the earlier work.

#### 5. PROJECTED ROTATIONAL VELOCITIES

We used a method developed previously (Penny 1996) to estimate the individual projected rotational velocities of the component stars from their CCFs with a narrow-lined star. For HD 135240, we used  $\tau$  Sco (HD 149438) as our tem-

plate star. As in the study above, we calibrated the relationship between the CCF Gaussian standard deviation  $\sigma$  and  $v \sin i$  using the Conti & Ebbets (1977) data sample. The resulting calibration curve is given by

$$v \sin i = (-7.8161 \times 10^{-3})\sigma^2 + 3.548\sigma - 111.1. \quad (1)$$

The fitted Gaussian widths of  $\sigma = 92.4 \pm 4.2$ ,  $88.4 \pm 9.8$ , and  $81.4 \pm 14.4$  km s $^{-1}$  for the primary, secondary, and tertiary correspond to projected rotational velocities of  $v \sin i = 150 \pm 9$ ,  $141 \pm 20$ , and  $126 \pm 31$  km s $^{-1}$ , respectively. While our primary value agrees with that of ST93 ( $150 \pm 10$  km s $^{-1}$ ), our secondary value is smaller than theirs ( $160 \pm 10$  km s $^{-1}$ ). We attribute this again to our treatment of the tertiary which was not considered by ST93. We note that Howarth et al. (1997) used *IUE* spectra to determine  $v \sin i$  values for this system of 146 and 103 km s $^{-1}$  for the primary and secondary.

#### 6. TOMOGRAPHIC RECONSTRUCTION AND SPECTRAL CLASSIFICATION

The separate spectra of all three stars can be derived using a tomography algorithm to reconstruct the individual spectra from the ensemble of composite spectra. The algorithm is described in detail in a separate paper (Bagnuolo et al. 1994), and its application in reconstructing the spectra of the triple-star system, 55 Uma, is described by Liu et al. (1997). We have commented on some limitations of the algorithm previously (Thaller et al. 1995), but we note here that strong wind features, such as the P Cygni lines, may be reconstructed incorrectly since their radial velocity curves can be very different from those associated with the stars themselves. Since the tomographic reconstruction is based on orbital Doppler shifts, the reconstruction will be ambiguous in the vicinity of such wind features.

The eclipsing nature of HD 135240 presents a complication in the tomographic reconstruction. The tomography algorithm assumes that the individual spectra contribute the same flux fraction in all the observed spectra. Thus, we only used spectra taken during phases outside of eclipse, and this amounted to 37 composite spectra which were used in the reconstruction.

The tomographic reconstruction of the component spectra is also based on assumed flux ratios which may not be well determined at the outset. We assume a constant value for the flux ratio over the 1200–1900 Å range, which is a reasonable assumption as long as this range corresponds to the Rayleigh-Jeans portion of the spectral distribution for each component (satisfied for stars earlier than B1 V which have a Wien peak below 1200 Å). The composite spectra are first separated using the CCF intensity ratios as initial estimates of the UV flux ratio. The resultant individual stellar spectra are then classified using the spectral diagnostics listed below. In our earlier work (Penny et al. 1997) we used the estimated classifications in a numerical scheme to determine the true UV flux ratios from the CCF intensity ratios. This approach becomes unduly complicated in triple-star applications, so here we opted for a variation of the method of Petrie (1939) of determining flux ratios through a comparison of the line depths of the reconstructed and standard, single-star spectra. Three single stars were selected with comparable classifications and projected rotational velocities to the three components of  $\delta$  Cir, their *IUE* spectra were processed and averaged together, and

finally the standard spectra were shifted into alignment with their respective reconstructed spectra. Then we used a non-linear least-squares routine to determine flux ratios,  $r_2 = F_2/F_1$  and  $r_3 = F_3/F_1$ , through a comparison of line depths in the reconstructed and standard spectra (omitting the broadlined regions near Ly $\alpha$  and the wind lines). The procedure solved for these two ratios subject to the constraint that the fractional contributions of the components summed to unity. The S/N is poor in the reconstructed secondary and tertiary spectra, so we smoothed the spectra of both the reconstructions and the standard spectra prior to fitting (this has the extra advantage of minimizing differences in line broadening). Table 4 lists the results of three trial comparisons using different sets of standard stars. The weighted mean results are UV flux ratios of  $r_2 = 0.239 \pm 0.022$  and  $r_3 = 0.179 \pm 0.021$ . We computed our final versions of the reconstructed spectra using these ratios.

Our method for estimating the spectral types and luminosity classes of the binary is based on the equivalent-width measurements of several UV absorption lines (see Penny, Gies, & Bagnuolo 1996 for details). We classify the primary and secondary as O7 III–V (O6.5–O7.5) and O9.5 V (O9–B0) based on an evaluation of the following criteria: for the primary, the equivalent widths of seven lines (Si III  $\lambda$ 1299, Fe V  $\lambda$ 1429, Fe IV  $\lambda$ 1567, He II  $\lambda$ 1640, Fe IV  $\lambda$ 1681, Fe IV  $\lambda$ 1723, Fe IV  $\lambda$ 1765) and the line ratios of He II  $\lambda$ 1640/Fe V  $\lambda$ 1429 and Fe IV  $\lambda$ 1723/Fe V  $\lambda$ 1429; and for the secondary the same set excluding the lines Fe IV  $\lambda$ 1567, 1765.

The third component is almost certainly an early B-type star, and, unfortunately, our classification scheme cannot be extrapolated into the B types. Instead, we estimated the classification of the tertiary using criteria described by Rountree & Sonneborn (1993). The reconstructed tertiary spectrum, although noisy, shows clear evidence of the Si III  $\lambda$ 1299 complex and possibly weak lines of Si II  $\lambda$ 1264, 1310 which suggests the type is B0.5 V or later. On the other hand, the N IV  $\lambda$ 1718 line is still present in the tertiary spectrum, which indicates a type earlier than B1 V, and thus, we adopt a classification of B0.5 V (B0–B1). We plan to present digital versions for this and the other O binaries in a future atlas of reconstructed spectra.

These classifications are, for the most part, consistent with Walborn’s (1972) composite classification of O7.5 III ((f)). We note that the N IV  $\lambda$ 1718 line that we use for luminosity classification purposes appears to more closely match that of an O7 V, but there is only a small difference in the strength of this profile from the dwarf to the giant class

at this subtype. Using our UV classification scheme, the earliest subtype at which we can detect a class III is O6.5, and there is significant scatter at the O7 subtype as well. Given these restrictions, it is clear that a giant luminosity class for the primary is possible. In fact, the absorption trough of the P Cygni–shaped C IV  $\lambda$ 1550 doublet appears to reach zero intensity in the summed composite spectrum (after allowance is made for the flux contributions of the secondary and tertiary), and this degree of absorption is only found in giants and brighter among O7 stars (Walborn, Nichols-Bohlin, & Panek 1985). Thus, we adopted a final primary classification of O7 III–V to indicate the uncertainty more than an intermediate luminosity class [note that Walborn’s suffix “((f))” is based solely on optical criteria and cannot be addressed here]. These spectral types correspond to temperatures of  $T_{\text{eff}, p} = 37.5 \pm 1.5$  kK,  $T_{\text{eff}, s} = 33 \pm 1.0$  kK (Howarth & Prinja 1989), and  $T_{\text{eff}, t} = 29 \pm 2$  kK (Underhill et al. 1979).

## 7. LIGHT-CURVE ANALYSIS AND MASSES

The discovery by *Hipparcos* (Perryman 1997) that HD 135240 is an eclipsing binary provides an opportunity to measure the system inclination and hence the component masses. The *Hipparcos* light curve is reproduced in Figure 4 as a function of photometric orbital phase where phase 0 is redefined to be the center of the primary eclipse (primary star superior conjunction). These phases were determined using our values for  $P$ ,  $T$ ,  $e$ , and  $\omega$  (photometric phase 0 corresponds to spectroscopic phase 0.48). The *Hipparcos* light curve shows two equally spaced minima of 0.14 and 0.15 mag in the *Hipparcos* magnitude system. It also displays an ellipsoidal variation due to the tidal distortion of the stars. The shapes and depths of the eclipses and the amplitude of the ellipsoidal variation are all dependent on the stellar radii and orbital inclination, and here we present model light-curve results that yield estimates of these important parameters.

We used the light-curve synthesis code GENSYN (Mochacki & Doughty 1972) to produce model  $V$ -band differential light curves (almost identical to differential *Hipparcos* magnitudes for hot stars). The code was written for binaries with circular orbits, and we used multiple runs to synthesize the varying orbital separation in an elliptical orbit (see Penny et al. 1999). Our approach was to make a constrained fit using as many data as possible from the spectroscopic results given above. The orbital parameters were taken from the spectroscopic solution, and the physi-

TABLE 4  
STANDARD SPECTRA AND FLUX RATIO ESTIMATES

Component	Name	Classification	$v \sin i$ (km s <sup>-1</sup> )	$r_2$	$r_3$
Primary .....	HD 36879	O7 V(n)	160		
Secondary .....	HD 116852	O9 III	130	0.232(37)	0.158(34)
Tertiary .....	HD 144470	B1 V	110		
Primary .....	HD 157857	O6.5 III(f)	114		
Secondary .....	HD 143275	B0.3 IV	150	0.247(39)	0.211(37)
Tertiary .....	HD 22951	B0.7 V	108		
Primary .....	HD 36879/157857 <sup>a</sup>	...	...		
Secondary .....	HD 34078	O9.5 V	141 <sup>b</sup>	0.239(39)	0.171(39)
Tertiary .....	HD 149438	B0.2 V	126 <sup>b</sup>		

<sup>a</sup> Shifted into coincidence and averaged.

<sup>b</sup> Artificially broadened for comparison purposes.

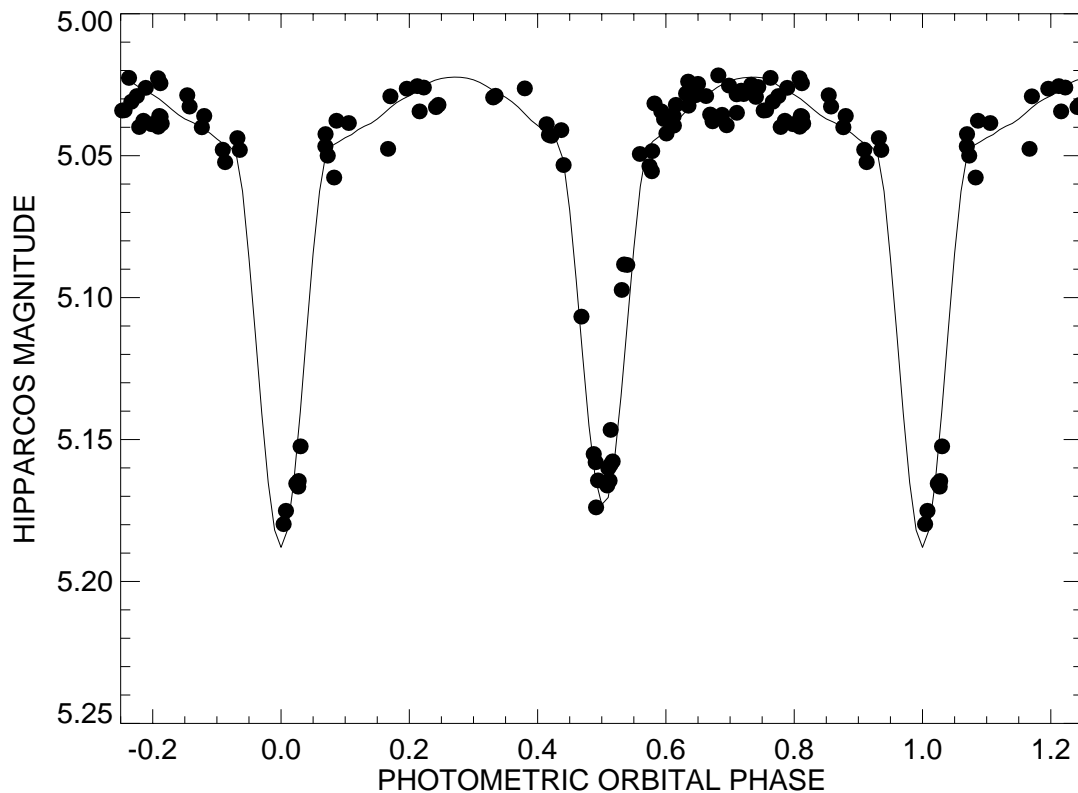


FIG. 4.—Observed *Hipparcos* light curve (filled circles) plotted together with the best-fit model (solid line)

cal parameters were estimated from the spectral classifications of the stars. We set the stellar temperatures and gravities according to the spectral classification calibration of Howarth & Prinja (1989;  $T_{\text{eff},p} = 37.5$ ,  $T_{\text{eff},s} = 33.0$  kK). We then estimated the physical fluxes and limb darkening coefficients from tables in Kurucz (1994) and Wade & Rucinski (1985), respectively. We also used the Kurucz flux models to transform our observed FUV flux ratio into a  $V$ -band flux ratio,  $F_s/F_p = 0.27 \pm 0.05$ . The theoretical and observed flux ratios together yield an estimate of the ratio of stellar radii. Then, for a given input value of the polar radius of the primary  $R_p$ , we calculated the secondary radius and spin rate (using the projected rotational velocities given above). Each trial run of GENSYN was set by two independent parameters, the system inclination  $i$  and primary polar radius. All the resulting light curves were corrected for the presence of third light using a visual flux ratio  $F_t/(F_s + F_p) = 0.16 \pm 0.05$ .

The first characteristic that we needed to match is the observed difference in eclipse depths. In a circular orbit this difference is entirely dependent on the difference in temperature between the component stars. However, in the case of HD 135240, the situation is slightly more complicated. Since  $\omega \approx 270^\circ$ , the secondary eclipse occurs approximately at periastron (and primary eclipse at apastron). This has the effect of reducing the depth (but widening the width) of the primary eclipse, with the opposite effect on the secondary eclipse. Using our first estimates of temperature from above, we found it impossible to match correctly both the primary and secondary depths in the same model. The secondary eclipse was deeper than the primary eclipse for all trial inclinations. The disagreement can be resolved by reducing the eccentricity and/or increasing the temperature difference

between stars. We found, however, that reducing the eccentricity by  $1 \sigma$  made little improvement, and so we focused instead on adjustments in temperature. We revised the assumed secondary temperature downward to  $T_{\text{eff},s} = 30$  kK which corresponds approximately to the lower limit consistent with acceptable range in spectral type (see above), and this led to satisfactory agreement between the model and observed differences in eclipse depths.

The separation in time of the two eclipses depends on  $e$  and  $\omega$ . The eclipses are nearly equally separated for  $\omega \approx 270^\circ$ , and we found that a slight adjustment in  $\omega$  from  $276^\circ$  to  $275^\circ$  led to a better match of the spacing of the eclipses.

There are three additional characteristics of the light curve that we sought to match: eclipse depth, eclipse duration, and amplitude of the ellipsoidal variation. The smaller the inclination, the larger the radius required to match the observed eclipse depths, and the minimum inclination acceptable (for a Roche filling primary) is  $i > 60^\circ$ . On the other hand, the ellipsoidal variations are a sensitive function of the assumed stellar radii, and we found that models with the correct ellipsoidal variation *and* eclipse duration had inclinations  $71^\circ < i < 77^\circ$ . The nominal, best-fit model light curve (for  $i = 74^\circ$ ) is illustrated in Figure 4. Refinements in the fit are unwarranted at present because of the limitations in phase coverage and the noise in the *Hipparcos* photometry.

This preliminary study of the light curve suggests that  $i = 74^\circ \pm 3^\circ$ . In all the model light curves (except that for  $i = 60^\circ$ , see above) both stars are *well* within their Roche limits. The polar radii for the best-fit inclination are  $R_p/R_\odot = 10.2 \pm 1.0$  and  $R_s/R_\odot = 6.4 \pm 0.7$ , and the average combined absolute magnitude of the pair is  $M_V =$

$-5.2 \pm 0.2$ . The equatorial rotation speeds of the two stars are  $156$  and  $147 \text{ km s}^{-1}$ . At these speeds the primary is rotating almost synchronously with the orbit, while the secondary has an angular rotational velocity that is approximately 70% faster than its orbital angular velocity at periastron.

#### 8. PLACEMENT IN THE H-R DIAGRAM AND DISCUSSION

Our goal in this research is to compare the masses obtained from observations with those found from theoretical evolutionary tracks. The observational masses are determined by combining results from the spectroscopic and photometric analyses ( $m \sin^3 i$  and  $i$ ). Masses from evolutionary theories require placing the individual component stars in the H-R diagram. We estimate temperatures from calibrations of spectral type, and we calculate luminosities from the observed flux ratio, the absolute magnitude of the binary (from the light-curve analysis), and associated bolometric corrections (Penny et al. 1997).

The spectral type-temperature calibration for O-type stars remains controversial (Hilditch, Harries, & Bell 1996; Penny et al. 1999). We list in Table 5 the range of assigned effective temperatures based on the calibrations of Vacca, Garmany, & Shull (1996, hereafter VGS), Howarth & Prinja (1989, hereafter HP), and Böhm-Vitense (1981, hereafter BV). If the “hotter” and “cooler” temperatures from the VGS and BV calibrations are adopted in the light-curve

models, the sizes and temperature differential of the two stars remain the same, but the resulting composite absolute magnitude changes by approximately  $\pm 0.1$  mag. This error is smaller than the range in absolute magnitude in the solution space of the light-curve analysis. We found in earlier work on binaries in clusters (Penny et al. 1997, 1999) that adoption of the HP temperature scale led to the best consistency in absolute magnitude estimates, and so we will use the HP temperatures ( $T_{\text{eff},p} = 37.5$  and  $T_{\text{eff},s} = 30.0$  kK) in what follows.

Individual visual magnitudes of the component stars were obtained from the visual flux ratio of the two stars,  $r_V = 0.27 \pm 0.05$ , and the adopted binary absolute magnitude,  $M_V = -5.2 \pm 0.2$ . These were converted to bolometric magnitudes and luminosities with bolometric corrections from Howarth & Prinja (1989). The luminosities and associated radii derived are  $\log L_p/L_\odot = 5.30 \pm 0.05$ ,  $\log L_s/L_\odot = 4.49 \pm 0.07$ ,  $R_p/R_\odot = 10.7 \pm 1.1$ , and  $R_s/R_\odot = 6.6 \pm 0.8$ . Our results are plotted in the H-R diagram in Figure 5 together with evolutionary tracks for single massive stars from Schaller et al. (1992). The position of the stars on the evolutionary tracks implies masses (and ages) of  $M_p/M_\odot = 32.7 \pm 2.5$  ( $2.5 \pm 0.9$  Myr) and  $M_s/M_\odot = 15.8 \pm 1.0$  ( $5.1 \pm 2.7$  Myr). Combining the light-curve model with the results from the spectroscopic orbit results in observational masses of  $M_p/M_\odot = 21.6 \pm 2.0$  and  $M_s/M_\odot = 12.4 \pm 1.0$ . The evolutionary masses are larger than those we derive from the orbit and light curve, and the disagreement is worst for the primary whose evolutionary mass is 50% larger than the mass we find.

It is possible that part of the discrepancy stems from outstanding problems related to the treatment of the third star in our analysis. The mass function from the spectroscopic orbit that determines the mass of the primary star depends critically on the semiamplitude of the secondary

TABLE 5  
EFFECTIVE TEMPERATURE ESTIMATES (kK)

Star	$T_{\text{eff}}(\text{VGS})$	$T_{\text{eff}}(\text{HP})$	$T_{\text{eff}}(\text{BV})$
Primary .....	$39.9 \pm 1.4$	$37.5 \pm 1.5$	$37.5^{+0.8}_{-1.3}$
Secondary .....	$34.6 \pm 1.3$	$33.0 \pm 1.0$	$32.4^{+1.2}_{-1.4}$

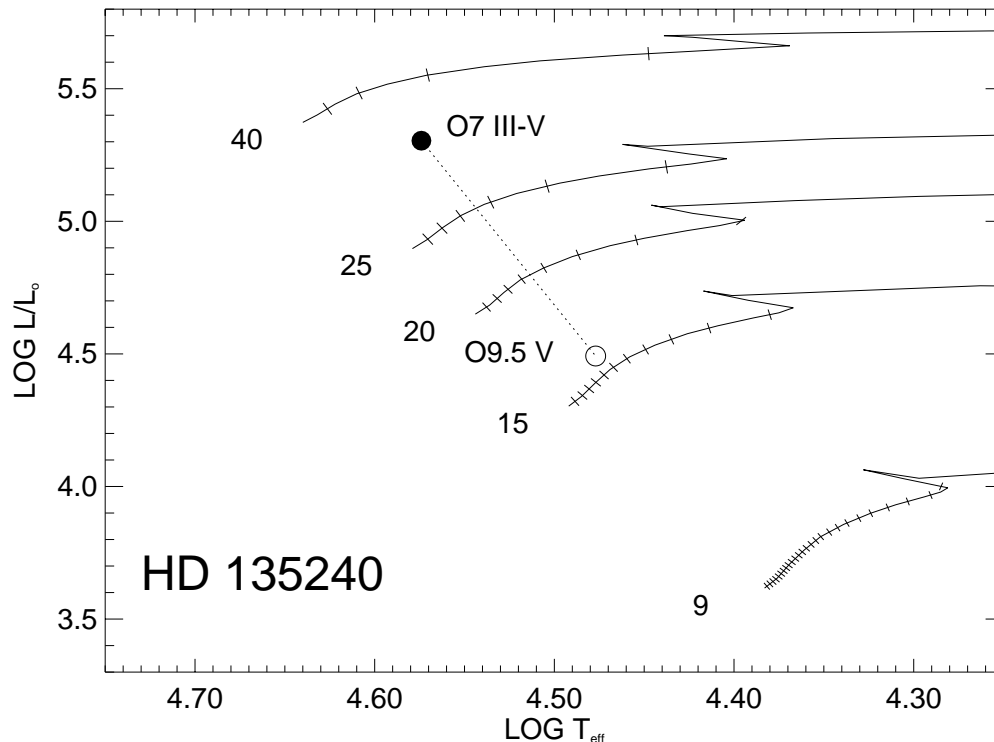


FIG. 5.—H-R diagram of the binary system HD 135240. The filled (open) circles represent the primary (secondary). The overdrawn evolutionary tracks are from Schaller et al. (1992) and are marked with ticks at each  $10^6$  yr in age. Each track is labeled with its zero-age main-sequence mass (in  $M_\odot$ ).

(varying as  $K_2^3$ ). In order for  $M_p$  to equal the evolutionary mass of  $32.7 M_\odot$ ,  $K_2$  would need to be  $320 \text{ km s}^{-1}$  or 19% larger ( $52 \text{ km s}^{-1}$ ) than our current estimate. It is interesting to note that if this were the value of  $K_2$  (and  $K_1$  remained the same), then the mass of the secondary from the orbital analyses would increase to  $15.6 M_\odot$  (because of the change in mass ratio), which is almost exactly the mass predicted by the evolutionary tracks for the secondary. We noted earlier (§ 3) that our neglect of the line blending influence of the third component in H $\alpha$  might result in underestimation of  $K_2$  by  $20 \text{ km s}^{-1}$ . It is possible that our Gaussian representation of the third component in the *IUE* CCFs (§ 2) was either too weak or too narrow to fully account for the actual line blending effects. However, we note that the projected rotational velocity for the third star based on the tomographic reconstruction (done independently of any assumptions about the character of the third star's spectrum) is  $117 \text{ km s}^{-1}$  (using our cross-correlation methods with the standard  $\tau$  Sco) which is close to the value of  $126 \pm 31 \text{ km s}^{-1}$  derived from the width of our Gaussian CCF model of the third component. Thus, it is unlikely that the tertiary would bias the measurements used to determine  $K_2$  by an amount sufficient to explain the entire mass discrepancy.

There are several areas of uncertainty in our light-curve analysis. The depths of the eclipses are extremely dependent on the amount of third light present. If we have overestimated the contribution from the tertiary, the model eclipses would need to be shallower, resulting in a smaller inclination and larger orbital masses. Assuming the radii of the stars remained the same, the necessary inclination to reconcile the primary's mass estimates is  $57^\circ$ . Of course, we might have underestimated the tertiary's light contribution, in which case our orbital masses would be even smaller. Another problem with the light curve is poor sampling, especially during the primary eclipse. The width of this eclipse and its depth are difficult to gauge. (Also the secondary eclipse would benefit from more observations to determine the minimum light value.) If the eclipses are actually narrower than they appear in our model light curve, we would need to reduce the radii of the stars, their luminosities, and subsequently the masses obtained from the evolutionary tracks. It is certainly possible to imagine a situation where a combination of poor eclipse sampling and uncertainties about the contribution of third light have led us to overestimates of the inclination and absolute magnitude for the inner binary of HD 135240.

If the explanation for the disagreement between the primary mass estimates is not to be found in our orbital analyses, what is its source? A great deal has been written about the "mass discrepancy" in O stars and between the mass derived from spectroscopic diagnostics and that taken from

the H-R diagram position (Herrero et al. 1992; Vacca et al. 1996; Burkholder, Massey, & Morrell 1997; Harries & Hilditch 1998). However, the discrepancy between the two theoretical methods is typically largest in very luminous stars (Of types) and is small to negligible in late O dwarfs. It would certainly be unusual to find such a large disagreement in a fairly young O7 III–V star. Another explanation is that this is a post Roche lobe overflow (RLOF) system in which the primary has suffered extensive mass loss. However, the stars are not in RLOF at this point, and this explanation requires some scenario (not readily apparent) that would halt the RLOF and leave the stars with most (or all) of their atmospheres intact. It is interesting to note that in a comparable massive binary, V3903 Sgr (O7 V + O9 V), Vaz et al. (1997) found no discrepancy between evolutionary and orbitally determined masses.

In closing, we see several areas in need of work to help resolve the problem of the mass discrepancy in HD 135240. Certainly a spectroscopic study at longer wavelengths could be helpful in more closely identifying both the true spectral class of the tertiary and its orbital relationship to the inner binary. Also the *Hipparcos* light curve is lacking in data at several phases, most particularly during primary eclipse. New photometry would facilitate a more complete light-curve model. We certainly look forward to further work on this triple system.

We are grateful to the director and staff of *IUE* Observatory for their support of these observations. Some of the data presented in this paper were obtained from the Multi-mission Archive at the Space Telescope Science Institute (MAST). STScI is operated by the Association of Universities for Research in Astronomy, Inc., under NASA contract NAS 5-26555. Support for MAST for non-*HST* data is provided by the NASA Office of Space Science via grant NAG 5-7584 and by other grants and contracts. This research has also made use of the SIMBAD database, operated at CDS, Strasbourg, France, and the ESA *Hipparcos* and Tycho Catalogues. Institutional support for L. R. P. has been provided from the College of Charleston School of Sciences and Mathematics. Additional support for L. R. P. was provided by the South Carolina NASA Space Grant Program and NSF grant AST 95-28506. Support for this work at GSU was provided by NASA grant NAG 5-2979. Institutional support has been provided from the GSU College of Arts and Sciences and from the Research Program Enhancement fund of the Board of Regents of the University System of Georgia, administered through the GSU Office of the Vice President for Research and Sponsored Programs. We gratefully acknowledge all this support.

#### REFERENCES

- Bagnuolo, W. G., Jr., & Gies, D. R. 1991, *ApJ*, 376, 266  
 Bagnuolo, W. G., Jr., Gies, D. R., Hahula, M. E., Wiemker, R., & Wiggs, M. S. 1994, *ApJ*, 423, 446  
 Bagnuolo, W. G., Jr., Gies, D. R., & Wiggs, M. S. 1992, *ApJ*, 385, 708  
 Böhm-Vitense, E. 1981, *ARA&A*, 19, 295  
 Bohannan, B., & Garmany, C. D. 1978, *ApJ*, 223, 908  
 Burkholder, V., Massey, P., & Morrell, N. 1997, *ApJ*, 490, 328  
 Conti, P. S., & Ebbets, D. 1977, *ApJ*, 213, 438  
 Garhart, M. P., Smith, M. A., Turnrose, B. E., Levay, K. L., & Thompson, R. W. 1997, *International Ultraviolet Explorer New Spectral Image Processing System Information Manual, Version 2.0* (Greenbelt: NASA)  
 Gies, D. R., Bagnuolo, W. G., Jr., & Penny, L. R. 1997, *ApJ*, 479, 408  
 Hardorp, J., & Scholz, M. 1970, *ApJS*, 19, 193  
 Harries, T. J., & Hilditch, R. W. 1998, in *ASP. Conf. Ser. 131, Boulder-Munich II: Properties of Hot, Luminous Stars*, ed. I. D. Howarth (San Francisco: ASP), 401  
 Herrero, A., Kudritzki, R. P., Vilchez, J. M., Kunze, D., Butler, K., & Haser, S. 1992, *A&A*, 261, 209  
 Hilditch, R. W., Harries, T. J., & Bell, S. A. 1996, *A&A*, 314, 165  
 Howarth, I. D., & Prinja, R. K. 1989, *ApJS*, 69, 527  
 Howarth, I. D., Siebert, K. W., Hussain, G. A. J., & Prinja, R. K. 1997, *MNRAS*, 284, 265  
 Hutchings, J. B. 1976, *ApJ*, 203, 438  
 Kaper, L., Fullerton, A., Baade, D., de Jong, J., Henrichs, H., & Zaal, P. 1998, in *Cyclical Variability in Stellar Winds*, ed. L. Kaper & A. W. Fullerton (ESO Astrophys. Symp. Ser.; Berlin: Springer), 103

- Kurucz, R. L. 1994, CD-ROM 19, Solar Abundance Model Atmospheres for 0, 1, 2, 4, 8 km/s (Cambridge: SAO)
- Liu, N., et al. 1997, *ApJ*, 485, 350
- Mason, B. D., Gies, D. R., Hartkopf, W. I., Bagnuolo, W. G., Jr., ten Brummelaar, T., & McAlister, H. A. 1998, *AJ*, 115, 821
- Mochnecki, S. W., & Doughty, N. A. 1972, *MNRAS*, 156, 51
- Morbey, C., & Brosterhus, E. B. 1974, *PASP*, 86, 455
- Penny, L. R. 1996, *ApJ*, 463, 737
- Penny, L. R., Gies, D. R., & Bagnuolo, W. G., Jr. 1996, *ApJ*, 460, 906
- . 1997, *ApJ*, 483, 439
- . 1999, *ApJ*, 518, 450
- Perryman, M. A. C. 1997, *The Hipparcos and Tycho Catalogues* (ESA SP-1200; Noordwijk: ESA)
- Petrie, R. M. 1939, *Publ. Dom. Astrophys. Obs. Victoria*, 7, 205
- Rountree, J., & Sonneborn, G. 1993, *Spectral Classification with the International Ultraviolet Explorer: An Atlas of B-Type Spectra* (NASA RP-1312; Washington, DC: NASA)
- Schaller, G., Schaerer, D., Meynet, G., & Maeder, A. 1992, *A&AS*, 96, 269
- Slettebak, A., Collins, G. W., II, Parkinson, T. D., Boyce, P. B., & White, N. M. 1975, *ApJS*, 29, 137
- Stickland, D. J. 1997, *Observatory*, 117, 37
- Stickland, D. J., Koch, R. H., Pachoulakis, I., & Pfeiffer, R. J. 1993, *Observatory*, 113, 139 (ST93)
- Stickland, D. J., Lloyd, C., Koch, R. H., Pachoulakis, I., & Pfeiffer, R. J. 1992, *Observatory*, 112, 150
- Thackeray, A. D., & Emerson, B. 1969, *MNRAS*, 142, 429
- Thaller, M. L. 1997, *ApJ*, 487, 380
- Thaller, M. L., Bagnuolo, W. G., Jr., Gies, D. R., & Penny, L. R. 1995, *ApJ*, 448, 878
- Underhill, A. B., Divan, L., Prévot-Burnichon, M.-L., & Doazan, V. 1979, *MNRAS*, 189, 601
- Vacca, W. D., Garmany, C. D., & Shull, J. S. 1996, *ApJ*, 460, 914
- Vaz, L. P. R., Cunha, N. C. S., Vieira, E. F., & Myrrha, M. L. M. 1997, *A&A*, 327, 1094
- Wade, R. A., & Rucinski, S. M. 1985, *A&AS*, 60, 471
- Walborn, N. R. 1972, *AJ*, 77, 312
- Walborn, N. R., Nichols-Bohlin, J., & Panek, R. J. 1985, *International Ultraviolet Explorer Atlas of O-Type Spectra from 1200 to 1900 Å* (NASA RP-1155; Washington, DC: NASA)